ACTA ACUSTICA UNITED WITH ACUSTICA
Vol. 90 (2004) 537 – 547

Modelling the Mechanical Response of the Reed-Mouthpiece-Lip System of a Clarinet. Part I. A One-Dimensional Distributed Model

Federico Avanzini
University of Padova, Department of Information Engineering, Via Gradenigo 6/A, 35131 Padova, Italy.
avanzini@dei.unipd.it

Maarten van Walstijn
Queen's University Belfast, Sonic Arts Research Centre, University Road, Belfast BT7 1NN, Northern Ireland.
m.vanwalstijn@qub.ac.uk

Summary
The motion of a clarinet reed that is clamped to a mouthpiece and supported by a lip is simulated in the time-domain using finite difference methods. The reed is modelled as a bar with non-uniform cross section, and is described using a one-dimensional, fourth-order partial differential equation. The interactions with the mouthpiece lay and the player's lip are taken into account by incorporating conditional contact forces in the bar equation. The model is completed by clamped-free boundary conditions for the reed. An implicit finite difference method is used for discretising the system, and values for the physical parameters are chosen both from laboratory measurements and by accurate tuning of the numerical simulations. The accuracy of the numerical system is assessed through analysis of frequency warping effects and of resonance estimation. Finally, the mechanical properties of the system are studied by analysing its response to external driving forces. In particular, the effects of reed curling are investigated.

PACS no. 43.75.Pq

1. Introduction

Research in musical acoustics has so far provided considerable insight in the functioning of the reed in single reed woodwind instruments. It is well understood that the reed behaves as a pressure controlled, inward-striking valve that tends to close when the mouth pressure p_m provided by the player is larger than the pressure p inside the mouthpiece.

The reed dimensions are small with respect to typical wavelengths in the resonator, thus pressure can be thought of as constant along the reed internal surface; under normal playing conditions, the first mode of the reed-mouthpiece-lip system is well above the main frequency component of the pressure difference signal that drives it; oscillations occur mainly in the vertical direction, and as a first approximation a single degree of freedom can be assumed. Based on these considerations, many authors have approximated the reed as a lumped second-order mechanical oscillator, driven by the pressure drop between mouth and mouthpiece.

Received 22 March 2002,
accepted 22 January 2004.

Backus [1] found experimentally an empirical non-linear equation relating the airflow through the mouthpiece slit to the pressure drop and the tip opening. Worman [2] was the first to formalise a complete non-linear theory. Such theory has been shown to account for many distinctive features of the system, such as the existence of a threshold blowing pressure and the occurrence of self-sustained oscillations [2, 3], as well as mode locking in a slightly inharmonic acoustical bore [4]. Wilson and Beavers [5] developed a theoretical analysis of operating modes of a clarinet by coupling a model similar to Worman's with an idealised cylindrical resonator, and showed qualitative agreement between theory and experiment. Schumacher [6] coupled the same kind of model to a realistic clarinet bore, described by its reflection function, and was able to compute transient and steady-state oscillations of the mouthpiece pressure via time-domain simulations. More recent research has questioned the validity of Backus' empirical equation; Hirschberg and coworkers [7, 8] adopted a flow model that uses the standard Bernoulli equation, and experiments by Gilbert [9] did not confirm Backus' findings. Dalmont *et al.* [10] have provided qualitative validation of the theory in [8].

A major limitation of lumped models is that a single degree of freedom with constant parameters can only be assumed for oscillations at small amplitudes. At larger am-

plitudes the reed *bends* against the mouthpiece lay, and the parameters of the lumped model can no longer be assumed constant. Furthermore, the phenomenon of reed beating (i.e. complete closure of the reed) is usually incorporated in the lumped model in a non-physical way, by imposing a maximum allowed displacement for the reed tip. Also, the dependence of the reed-mouthpiece system on the lip embouchure is not taken into account in a lumped representation.

A distributed representation of the reed is that of a bar with non-uniform cross-sectional area, clamped to the mouthpiece at one end. Additional constraints on the reed motion are provided by the mouthpiece profile and interaction with the lip. Stewart and Strong [11] developed a numerical model based on such a distributed description, which incorporated automatically bending and beating phenomena. Later, Sommerfeldt and Strong [12] used the same model for studying a player-clarinet system where the player's air column was also included in the simulations. The distributed modelling approach was also adopted by Gilbert [9] and Gazengel [13], who provided analytical studies of reed bending in the case of simplified geometries (wedge shaped reed, circular lay profile) and proposed a method for designing a lumped model approximation with non-constant parameters.

Distributed modelling of the reed-mouthpiece-lip system is also the topic of this paper. The modelling principles presented here are similar to those adopted in [11, 12], but contain several improvements and refinements. The fourth-order partial differential equation (*PDE*) describing the reed is adapted in a such way that internal losses and damping due to the surrounding air, as well as the physical interaction with the mouthpiece lay and the player's lips, are modelled more accurately. The equations are discretised using an implicit finite-difference scheme that guarantees unconditional stability and minimum frequency warping in the digital domain. This numerical technique was already used by Chaigne and Doutaut [14] for the modelling of idiophones.

Being one-dimensional, the distributed model described in this paper cannot account for torsional modes in the reed oscillation. In order to simulate the presence of torsional modes, as indicated in recent works by Ducasse [15] and by Facchinetti *et al.* [16], two- or three-dimensional distributed models would be needed. This issue is not addressed here, and future research is required to investigate the influence of the torsional modes on the reed-lay-mouthpiece system. Moreover, no attempt is made here to model the air flow in the reed channel or to simulate the acoustical resonator. Instead attention is exclusively focused on the mechanical response of the reed-mouthpiece-lip system. Both geometrical and mechanical parameters are either obtained via precise measurements on real clarinet mouthpieces or fine-tuned via numerical simulations.

The remainder of the paper is structured as follows: section 2 describes the main features of the continuous-time model, including losses and reed-lay, reed-lip interactions; details of the numerical techniques are provided in section 3, while measurements of the model parameters are presented in section 4; finally, results from numerical simulations are found in section 5.

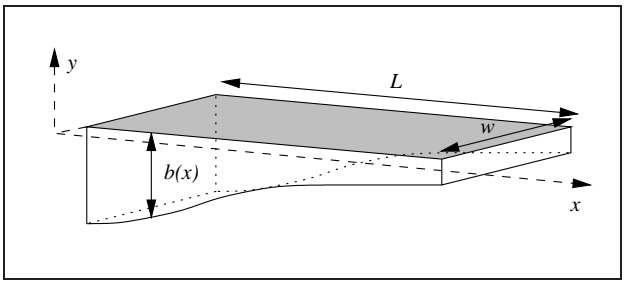

Figure 1. Geometry of a clarinet single reed.

2. The model

Section 2.1 describes the fourth-order PDE that is used for modelling the reed as a non-uniform clamped-free bar. Then, in section 2.2 the problem of the reed-lay, reed-lip interactions is addressed.

2.1. Reed

The reed is modelled here as a bar with length L, uniform width w and non-uniform thickness $b(x)$ (see Figure 1). It is clamped to the mouthpiece at one end ($x = 0$) and free at the other one ($x = L$). Only flexural waves in the vertical direction are considered, and contributions of longitudinal waves are neglected, as well as flexural waves in the horizontal plane. If the material is homogeneous and isotropic, then its density ρ and Young's modulus Y are constants, and the vertical displacement distribution $y(x,t)$ is governed by the equation

$$F(x,t) = \frac{\partial^2}{\partial x^2}\left[Y\, I(x)\left(1+\eta\,\frac{\partial}{\partial t}\right)\frac{\partial^2 y}{\partial x^2}(x,t)\right] + \rho S(x)\left[\frac{\partial^2 y}{\partial t^2}(x,t)+\gamma_B\frac{\partial y}{\partial t}(x,t)\right], \qquad (1)$$

where t is time and x is the horizontal position along reed length, $y(x,t)$ is the vertical position of the top-surface of the reed (where $y = 0$ when the reed is clamped on the mouthpiece and undisturbed by lip and other forces), $S(x)$ denotes the cross-section, while $F(x,t)$ is a driving force per unit length. The term $I(x) = S(x)\kappa^2(x)$ is the moment of inertia about the longitudinal axis, where $\kappa(x)$ is the radius of gyration of the cross-section $S(x)$. If a rectangular cross-section is assumed, then $S(x) = wb(x)$ and $\kappa(x) = b(x)/\sqrt{12}$. Note that equation (1) holds only if $S(x)$ is a slowly varying function [17]. The coefficient η represents the magnitude of the internal viscoelastic losses, and γ_B accounts for damping of the surrounding fluid. Chaigne and Doutaut [14] have shown that these two coefficients yield a satisfactory representation of bar losses. In particular, they found that the frequency-

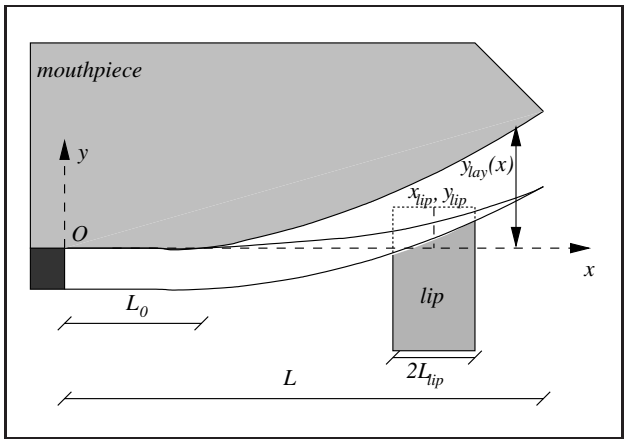

Figure 2. Geometrical parameters for the mouthpiece lay and the lip.

dependent damping factor $\alpha(f)$ of the bar is fairly well fitted by the empirical law

$$\alpha(f) = \frac{1}{t_d(f)} = a_0 + a_2 f^2, \tag{2}$$

where t_d is the decay time. It is shown in [14] that the $a_{0,2}$ coefficients are related to η, γ_B through the formulae

$$\eta = a_2/2\pi^2 \quad \text{and} \quad \gamma_B = 2a_0. \tag{3}$$

Finally, clamped-free boundary conditions lead to the constraints (see for instance [18])

$$y(0,t) = \frac{\partial y}{\partial x}(0,t) = 0,$$
$$\frac{\partial^2 y}{\partial x^2}(L,t) = \frac{\partial^3 y}{\partial x^3}(L,t) = 0. \tag{4}$$

2.2. Interaction with the mouthpiece and the lip

Besides clamping at the mouthpiece, additional constraints on the reed motion are the support provided by the player's lip, and the interaction with the mouthpiece lay. A simple approach, which was adopted in [11, 12], is to model an inelastic collision by imposing a "stop": when a collision between the reed and the lay is detected at a certain point x, the reed velocity $\dot{y}(x,t)$ is set to zero and the displacement $y(x,t)$ is kept constant as long as the reed point tends to move into the mouthpiece. This approach introduces artificial accelerations in the system. Imposing a stop on a reed point means immediately adding forces also on the neighbouring points, which are not necessarily in contact with the mouthpiece. Since these added forces cannot be explained or interpreted as contact, driving or shear forces, this approach is somewhat non-physical, and in many cases amounts to artificially affecting the accelerations of the reed sections.

The lip position is specified by the pair (x_{lip}, y_{lip}) as in Figure 2, where y_{lip} is the vertical position of the top of the lip when uncompressed. It is assumed that the reed and the lip are permanently in contact over a fixed segment $X_{lip} = (x_{lip} - L_{lip}, x_{lip} + L_{lip})$, and that there is an elastic lip force per unit length $F_{lip}(x,t)$ between them that is proportional to the lip compression:

$$F_{lip}(x,t) = \begin{cases} -K_{lip}\Delta y_{lip}(x,t) & x \in X_{lip}, \\ 0 & \text{otherwise}, \end{cases} \tag{5}$$

where $\Delta y_{lip}(x,t) = y_{lip} - y(x,t) + b(x)$ indicates lip compression and K_{lip} is the lip stiffness per unit length. Equation (5) provides the simplest possible restoring force, which is intended as a first-order approximation in the case of using an artificial lip (see section 4). Note that no lip restoring forces were modelled in [11, 12]. As a second effect, the lip provides additional damping to the reed. Following [12], we redefine the damping coefficient γ_B as position dependent:

$$\gamma_B(x) = \begin{cases} \gamma_{air} + \gamma_{lip} & x \in X_{lip}, \\ \gamma_{air} & \text{otherwise}. \end{cases} \tag{6}$$

Reed-lay interaction is slightly more complicated, since the portion of reed in contact with the mouthpiece varies over time. The lay is defined through its profile $y_{lay}(x)$, as in Figure 2 and the contact force per unit length is defined as $F_{lay}(x,t) = F_{el}(x,t) + F_{dis}(x,t)$, where F_{el} and F_{dis} are an elastic and a dissipative component, respectively. Suppose that a section dx of the reed around x is hitting the lay, i.e. $y(x,t) = y_{lay}(x)$. Since the collision is nearly inelastic [11], F_{dis} is chosen such that it nullifies the velocity of the section during the duration Δt of the collision. If Δt is short, from the law of impulsion we obtain

$$dm(x)\, \dot{y}(x,t) = \left[F_{dis}(x,t)dx\right]\Delta t, \tag{7}$$

where $dm(x) = \rho b(x) w\, dx$ is the mass of the reed section. Therefore F_{dis} is non-zero only during the time Δt in which collision occurs. Equation (7) will be exploited in section 3 for deriving an expression for F_{dis} in the discrete space-time domain.

The elastic term F_{el} is nonzero only if the reed section is still in contact with the lay after the collision. In this case, a linear elastic restoring force is applied, such that F_{el} takes the form

$$F_{el}(x,t) = \begin{cases} -K_{lay}\Delta y_{lay}(x,t) & \Delta y_{lay} > 0, \\ 0 & \text{otherwise}, \end{cases} \tag{8}$$

where $\Delta y_{lay}(x,t) = y(x,t) - y_{lay}(x)$. Again, note that contact forces with the lay were not modelled in [11, 12].

In conclusion, the force F in equation (1) is given by

$$F(x,t) = F_{lip}(x,t) + F_{lay}(x,t) + F_{ext}(x,t), \tag{9}$$

where the term F_{ext} stands for an external driving force per unit length.

3. Numerical formulation

3.1. Implicit θ-scheme

Equation (1) has to be discretised in both time and space. Finite-difference methods (*FDM*) approximate the spatial domain with a grid of N sections (equivalently, $N+1$ points), and a corresponding spatial sampling step $X_s = L/N$. The sampling step in time is $T_s = f_s^{-1}$, where f_s is the sampling rate. In the following the notation y_i^n is used to denote the value of the reed displacement y at the point $x_i = iX_s$ (for $i = 0 \ldots N$) and at time $t_n = nT_s$ (with $n \geq 0$); the vector notation $\boldsymbol{y}^n = [y_i^n]_i$ will also be used.

The selection of the two parameters X_s, T_s is usually imposed by stability and frequency warping criteria. *Explicit* FDM can be used, where discretisation of the derivatives leads to an explicit dependence of y_i^{n+1} on known quantities. It is a general result that if the PDE does not model any damping, explicit schemes lead to a Von Neumann stability condition of the form $T_s/X_s^2 < c$, where c is a constant [19]. This condition takes on a slightly different form when dissipative elements are included. Chaigne and Doutaut have shown that the stability condition for the numerical formulation of equation (1) with explicit methods can be written $N < N_{max}(f_s)$ i.e. the number of grid-points has an upper bound determined by the sampling rate. Moreover, it was shown in [14] that for a non-uniform bar modelled with equation (1) the function $N_{max}(f_s)$ is roughly proportional to $\sqrt{f_s}$ for low f_s, and tends to an asymptotic limit as f_s increases. Therefore, extremely high sampling rates should be used in order to achieve an acceptable spatial resolution, and consequently a reasonable estimation of the first natural frequencies of the bar.

For this reason we resort to a specific class of implicit schemes known as the "variable-weighted implicit approximation method" [19], and also referred to as θ-schemes. This method is described in the Appendix; here we recall that it is based on time-smoothing of the spatial derivatives, where the smoothing is controlled by the free parameter $0 \leq \theta \leq 1$. For values $\theta \geq 1/4$ the method is unconditionally stable, i.e. it is stable for any combination of X_s and f_s.

The notation Δ_i^n is used for defining the approximation of the spatial derivative term provided by the θ-scheme:

$$\frac{\partial^2}{\partial x^2}\left[I\left(1+\eta\frac{\partial}{\partial t}\right)\frac{\partial^2 y}{\partial x^2}\right](x_i,t_n) \approx \Delta_i^n. \qquad (10)$$

Then the difference equation is seen to take the form

$$(1+\gamma)\,y_i^{n+1} - 2y_i^n + (1-\gamma)\,y_i^{n-1} = \frac{T_s^2}{\rho S_i}\left[F_i^n - Y\Delta_i^n\right], \qquad (11)$$

where $\gamma = \gamma_B T_s/2$. Note that this equation is implicit, since the term Δ_i^n depends on y_i^{n+1}. In matrix form, the numerical system is:

$$\boldsymbol{M}_1\boldsymbol{y}^{n+1} = \boldsymbol{M}_0\boldsymbol{y}^n + \boldsymbol{M}_{-1}\boldsymbol{y}^{n-1} + \boldsymbol{M}_F\boldsymbol{F}^n. \qquad (12)$$

The coefficients of the matrices $\boldsymbol{M}_1$, $\boldsymbol{M}_0$, $\boldsymbol{M}_{-1}$ and $\boldsymbol{M}_F$ are found from the calculations outlined in the Appendix. Thus, computation of $\boldsymbol{y}^{n+1}$ requires inversion of the matrix $\boldsymbol{M}_1$, and the final numerical system has the form:

$$\boldsymbol{y}^{n+1} = \boldsymbol{A}_0\boldsymbol{y}^n + \boldsymbol{A}_{-1}\boldsymbol{y}^{n-1} + \boldsymbol{A}_F\boldsymbol{F}^n, \qquad (13)$$

where $\boldsymbol{A}_{[0,-1,F]} = \boldsymbol{M}_1^{-1}\boldsymbol{M}_{[0,-1,F]}$.

3.2. Computation of the contact force

The elastic lip force $(\boldsymbol{F}_{lip})^n$ and the elastic component of the lay forces $(\boldsymbol{F}_{el})^n$ are easily computed directly from equations (5) and (8), respectively. Computation of the dissipative force $(\boldsymbol{F}_{dis})^n$, assuming an inelastic collision, is less straightforward. As stated in section 2.2, $(F_{dis})_i^n$ is non-zero only when a collision occurs, therefore one first needs to find the sections i that are colliding with the lay at time n. To this end the next value $\hat{\boldsymbol{y}}^{n+1}$ for the displacement distribution is predicted from equation (13) using a force vector $(\hat{\boldsymbol{F}})^n$ that contains only lip and external forces. This gives a prediction of which sections i are going to collide with the mouthpiece lay using the condition

$$C_i^n: \ \left\{\hat{y}_i^{n+1} > (y_{lay})_i \text{ and } y_i^n < (y_{lay})_i\right\}. \qquad (14)$$

Moreover, those sections that are colliding with the lay have an estimated velocity

$$\hat{v}_i^n = \frac{\hat{y}_i^{n+1} - y_i^{n-1}}{2T_s}. \qquad (15)$$

From these equations and from equation (7) an expression for $\boldsymbol{F}_{dis}$ can be derived in discrete time:

$$(F_{dis})_i^n = \begin{cases} \dfrac{m_i}{T_s}\hat{v}_i^n & \text{if } C_i^n \text{ holds,} \\ 0 & \text{otherwise,} \end{cases} \qquad (16)$$

where $m_i = \rho b_i w$ is the mass per unit length of the i^{th} section. Note that equation (16) has been derived from equation (7) under the simplifying assumption that the reed section is stopped within a single time step T_s, i.e. the collision time Δt is shorter than T_s. In summary, an inelastic collision that is anticipated to commence within a certain sampling period T_s is modelled with a force F_{dis} that is constant over that period. The force value is chosen such that the total work done over T_s equals the work required to nullify the velocity.

Once $(\boldsymbol{F}_{dis})^n$ has been estimated, the next displacement $\boldsymbol{y}^{n+1}$ is recomputed from equation (12) using the force vector $\boldsymbol{F}^n$ that includes lay forces. At this point condition C_i^n must be re-evaluated for the displacement $\boldsymbol{y}^{n+1}$, since the subset of colliding sections may *a priori* have changed. In other words, reed-lay contact computation must be computed iteratively, until the evaluation of C_i^n converges to a stable configuration. Summarizing, at each time step n the new displacement $\boldsymbol{y}^{n+1}$ is computed as described in the following pseudocode lines:

for $n \geq 1$
  $\boldsymbol{F}_{dis}^n = 0$
  for $(j = 1 \ldots n_{dis}\,;\; j{+}{+})$
    Compute $\boldsymbol{F}^n = \boldsymbol{F}_{lip}^n + \boldsymbol{F}_{ext}^n + \boldsymbol{F}_{lay}^n$
    Estimate $\hat{\boldsymbol{y}}^{n+1} = \boldsymbol{A}_0 \boldsymbol{y}^n + \boldsymbol{A}_{-1} \boldsymbol{y}^{n-1} + \boldsymbol{A}_F \hat{\boldsymbol{F}}^n$
    Evaluate condition C_i^n and velocities $\hat{v}_i^n$
    Compute $\boldsymbol{F}_{dis}^n$
  end
  $\boldsymbol{y}^{n+1} = \hat{\boldsymbol{y}}^{n+1}$
end

Empirical observations on the numerical simulations have shown that the parameter n_{dis} does not affect the results significantly.

4. Measurements

In order to obtain meaningful results from the numerical simulation of the reed-mouthpiece-lip system, it is essential to establish accurate estimates of the model parameters. Not all the parameters are easily found via direct measurements, therefore some of them are estimated by adjusting their values while running numerical simulations until the behaviour is similar to that observed in real systems. Results are given in Table I, while measurement strategies are detailed in the remainder of the section. Note that our measurements on the reed and lay geometries differ significantly from those reported in [11, 12].

4.1. Geometrical parameters

A clarinet mouthpiece lay has a flat part at the end connected to the bore, where the reed is clamped. The remaining part is curved (see Figure 2). For three mouthpieces (namely, a Bundy, a Calteau and a Reginald Kell) we measured the total length of the lay L, the length of the flat part L_0 and the profile $y_{lay}(x)$. The latter was measured using a travelling microscope and the data-points were fitted with a fourth-order polynomial, with the additional constraints

$$y_{lay}(L_0) = 0 \quad \text{and} \quad \frac{dy_{lay}}{dx}(L_0) = 0, \tag{17}$$

in order to ensure a smooth connection to the flat part. As shown in Figure 3a, the three mouthpieces differ significantly in length and in curvature. The simulations described in the following sections use the Bundy mouthpiece data. For this mouthpiece the curved profile (in meters) is

$$\begin{aligned} y_{lay}(x) \;=\; & 1.6181(x-L_0)^2 + 1.8604(x-L_0)^3 \\ & + 5.5077 \cdot 10^2 (x-L_0)^4, \end{aligned} \tag{18}$$

for $x > L_0$. A plastic-coated reed was chosen instead of a cane reed, because its mechanical properties remain approximately constant independently of humidity (see section 4.2). In our approximation the reed is assumed to have a rectangular cross-section, as in Figure 1. This does not fully correspond to reality, since in real reeds the thickness

Table I. Parameters used in the simulations. The label **M** refers to parameter values established through direct measurements; **C** indicates that the value has been fine-tuned via numerical simulations.

Reed - (RICO plasticover, hardn. 2)		
Length (free part when clamped)	$L = 34 \cdot 10^{-3}\,\mathrm{m}$	**M**
Width	$w = 13 \cdot 10^{-3}\,\mathrm{m}$	**M**
Density	$\rho = 500\,\mathrm{kg/m^3}$	**M**
Young's Modulus	$Y = 5.6 \cdot 10^9\,\mathrm{N/m^2}$	**C**
Viscoelastic constant	$\eta = 6.0 \cdot 10^{-7}\,\mathrm{s}$	**C**
Fluid damping coefficient	$\gamma_{air} = 100\,\mathrm{s^{-1}}$	**C**
Mouthpiece (Bundy)		
Lay length (total)	$L = 34 \cdot 10^{-3}\,\mathrm{m}$	**M**
Lay length (flat part)	$L_0 = 9 \cdot 10^{-3}\,\mathrm{m}$	**M**
Contact stiffness per unit length	$K_{lay} = 10^8\,\mathrm{N/m^2}$	**C**
Artificial lip (water-filled balloon)		
Horizontal position	$x_{lip} = 22 \cdot 10^{-3}\,\mathrm{m}$	**M**
Vertical position	$y_{lip} = 3.85 \cdot 10^{-3}\,\mathrm{m}$	**C**
Length of the contact segment	$2L_{lip} = 9 \cdot 10^{-3}\,\mathrm{m}$	**M**
Stiffness per unit length	$K_{lip} = 6.5 \cdot 10^4\,\mathrm{N/m^2}$	**M**
Additional fluid damping	$\gamma_{lip} = 16000\,\mathrm{s^{-1}}$	**C**

b is not constant over the width w. Therefore both the minimum and the maximum reed thickness were measured at position x, and an "effective" thickness was computed under the hypothesis that the curvature over w has a circular shape. Measurements were taken at 18 points along the reed length, and the data-points were fitted again with a fourth-order polynomial. The thickness profile (in meters) of the plastic reed is

$$\begin{aligned} b(x) \;=\; & 2.2633 \cdot 10^{-3} - 4.9483 \cdot 10^{-2} x - 4.444 x^2 \\ & + 2.0126 \cdot 10^2 x^3 - 2.4385 \cdot 10^3 x^4. \end{aligned} \tag{19}$$

Both the measured points and the polynomial fit are shown in Figure 3b. When mounted on the Bundy mouthpiece, the total reed length from the clamping point to the tip is $L = 34 \cdot 10^{-3}\,\mathrm{m}$.

The horizontal coordinate of the lip x_{lip} and the length $2L_{lip}$ of the contact segment X_{lip} were chosen according to typical embouchures. Values are qualitatively in agreement with those used in [11, 12]. The value for the vertical coordinate y_{lip} was not specified a priori, instead it was chosen through numerical simulations: namely, y_{lip} was calibrated in such a way that the resulting rest tip position y_0 provided in the simulations a rest tip opening $y_{lay}(L) - y_0 = 4 \cdot 10^{-4}\,\mathrm{m}$.

4.2. Mechanical parameters

The determination of the mechanical parameters of the reed is less straightforward than the geometrical measurements.

Volume density ρ of the plastic reed was found by weighing the reed and dividing the result by the reed volume as given by geometrical measurements. Taking into account the error of the weighing machine that we used,

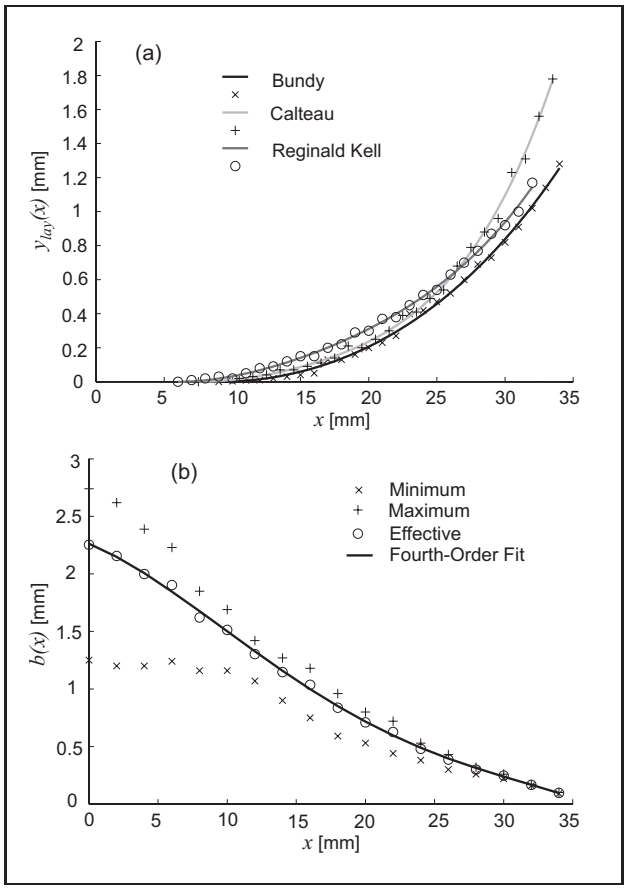

Figure 3. Geometrical parameters, measurements and polynomial fits; (a) three mouthpiece profiles $y_{lay}(x)$ and (b) reed profile $b(x)$.

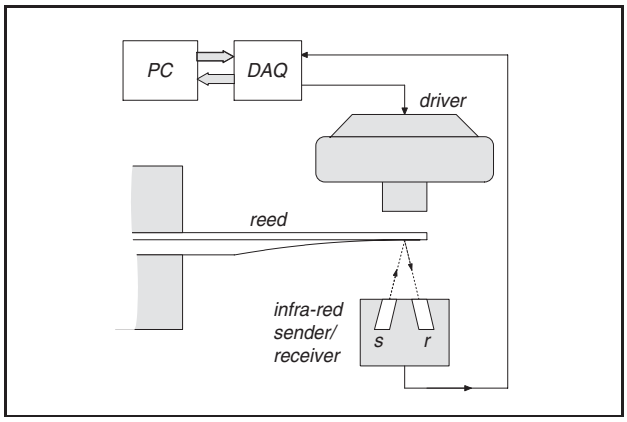

Figure 4. A picture of the experimental set-up used to determine Y, η, and γ_{air} (the label *DAQ* stands for Data Acquisition Board).

the density was found to lie in the interval $(459, 535)$ Kg/m^3, and the value $\rho = 500$ Kg/m^3 was arbitrarily chosen.

In order to determine the reed Young's modulus Y and the damping constants η and γ_{air}, experiments were carried out in an anechoic chamber, with the reed clamped between two perspex plates and a thin piece of hard rubber fitted in between on the curved side of the reed. A schematic picture of the experimental setup is provided in Figure 4. The reed was excited with a horn driver, and its responses were measured using an infra-red sender/receiver system placed on the other side of the reed. The experiment consisted of four steps.

1. The reed was simply plucked, and a rough estimation was made of the first two resonance frequencies $f_{1,2}$ via Fourier-transforming the reed response.
2. The reed was driven using a high-amplitude sinusoidal signal at the first mode frequency ($f_1 \sim 1.4$ kHz). The driving frequency was adjusted until the reed response reached a maximum, then the driving amplitude A_{max} was measured with a microphone. The damping factor of f_1 was estimated by measuring the decay pattern of the waveform after sudden suppression of the driving signal.
3. The reed was excited with driving frequency f_2 and driving amplitude A_{max}. The second mode is very strongly damped however, and it was found that the amplitude of the horn driver is insufficient for f_2 excitation that can be measured with the experimental setup.
4. The minimum amplitude A_{min} that is required to excite f_1 was measured. Taking into account the frequency-dependence of the microphone, $A_{max} - A_{min}$ was found to be about 32 dB. Given that the infra-red receiver system has a flat magnitude response in the frequency area of interest, it follows that the response at f_1 must be at least 32 dB stronger in amplitude than the response at f_2.

These experimental results were used to determine the reed Young's modulus Y and the damping constants η and γ_{air} in three steps.

1. Since the only unknown parameter which influences the location of f_1 is the Young's modulus Y, this parameter was adjusted in numerical simulations (without lip and lay interactions), until they exhibited the proper f_1 value.
2. Numerical simulations showed that the difference in amplitude between $f_{1,2}$ depends only on η, in accordance with equations (2) and (3). Figure 5 shows this dependence as found from the simulations. Since the amplitude difference between the two modes has to be at least 32 dB, the viscoelastic constant must be at least $\eta = 6 \cdot 10^{-7}$ s.
3. The fluid damping value γ_{air} was found to have approximately the same damping effect on all frequencies. Again, this is in accordance with equations (2) and (3). γ_{air} was then determined by adjusting it until simulations exhibited the same damping behaviour at f_1 as measured in the second experimental stage.

The mechanical properties of a human lip are not easily determined, therefore we estimated the elastic constant K_{lip} in equation (5) using an artificial lip set-up in the form of a balloon filled with water. This is justified to some extent by the fact that many authors have studied

clarinet vibrations using artificial lips in experimental setups [2, 20, 12, 21]. Several weights were placed together with a clarinet reed on the balloon and the corresponding lip compressions were measured using a travelling microscope. The stiffness per unit length K_{lip} was then estimated as the steepness of a linear fit to the data. The additional damping γ_{lip} defined in equation (6) was chosen by adjusting it until numerical simulations exhibited a damping behaviour similar to that observed by Worman [2], i.e. a half power bandwidth $g \approx 3000$ rad/s for the first mode f_1. Finally, K_{lay} in equation (8) was chosen empirically; its value is the highest that was observed not to lead to instability in numerical simulations.

An accurate determination of all the mechanical and geometrical parameters is difficult, which may explain discrepancies between model and experiments.

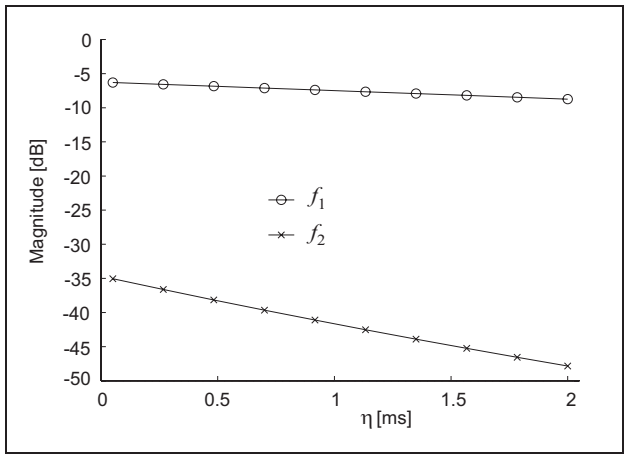

Figure 5. Dependence of the amplitude of $f_{1,2}$ on the viscoelastic constant η, as found with the numerical simulations.

5. Simulations

Numerical approximation always introduces errors in the simulations. This problem is addressed in section 5.1, where optimal values for the numerical parameters are chosen on basis of the analysis of frequency warping and resonance estimation. Sections 5.2 and 5.3 present the main results on the mechanical properties of the system, obtained from numerical simulations.

5.1. Numerical parameters

The numerical distributed model developed by Stewart and Strong [11] and Sommerfeldt and Strong [12] makes use of a θ-scheme with $\theta = 1/2$. However, Chaigne and Doutaut [14] have shown that, for a given number of sections N and sampling rate f_s, minimum frequency warping in the discrete-time system is obtained using $\theta = 1/4$.

We analysed impulse responses obtained from numerical simulations of a uniform bar (without lip and lay interactions) using values for θ between $1/4$ and $1/2$. For such a uniform geometry, the resonances f_i are known from theory, and simulations confirmed that $\theta = 1/4$ provides the best approximation to the theoretical values. Then impulse responses of the reed were analysed by running simulations with the non-uniform thickness of equation (19) and without lip and lay interactions. Estimation of the resonances through FFT analysis has shown that frequency warping starts to be significant above the first three resonances. In particular, $\theta = 1/4$ and $\theta = 1/2$ provide the same estimate $f_1 = 1405$ Hz for the first resonance, while the discrepancy in f_2 estimation is less than 1%. Nonetheless, these results confirm that $\theta = 1/4$ minimizes frequency warping effects also in the non-uniform case. This value is therefore used in the rest of the paper.

Another important numerical parameter is N, since it defines the spatial resolution and therefore affects the resonance estimation. In order to choose suitable values for f_s and N we resorted to analysis of convergence, i.e. analysis of resonance estimation in the numerical system with respect to f_s and N. Simulations were run with various

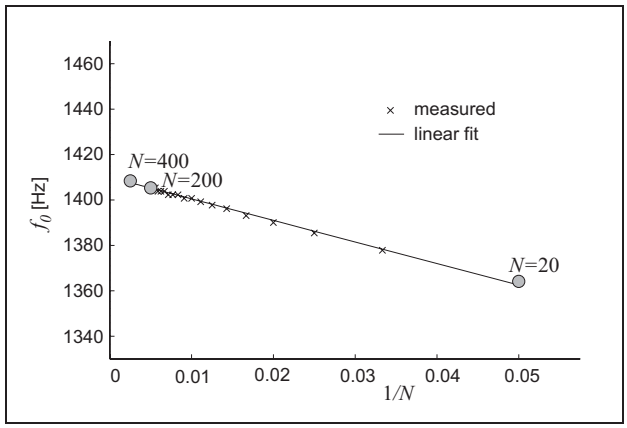

Figure 6. Analysis of convergence for f_1, with $f_s = 200$ kHz.

f_s and N, without lip and lay interactions. The first resonance f_1 of the system was obtained through FFT analysis. Higher resonances were not taken into account, since they are strongly damped and their estimation does not affect the system behaviour significantly.

Results are summarized in Table II: it can be noticed that the estimated values always converge with increasing N. Moreover, the columns with $f_s = 200$ kHz and $f_s = 400$ kHz provide the same estimated f_1 values for every N. Figure 6 shows the convergence analysis for $f_s = 200$ kHz and varying N. Again, it can be seen that f_1 converges for increasing N. Moreover, the estimate with $N = 200$ is very close to that found with $N = 400$, the discrepancy being 0.2%. From these results it is concluded that the values $f_s = 200$ kHz and $N = 200$ provide sufficiently accurate simulations. These values are therefore used in the rest of the paper.

5.2. Dynamic and quasi-static simulations

Using the numerical parameters as determined in the last section, simulations of the complete system were run both in a *dynamic* and in a *quasi-static* manner. Dynamic simulations were obtained by driving the system with a sinu-

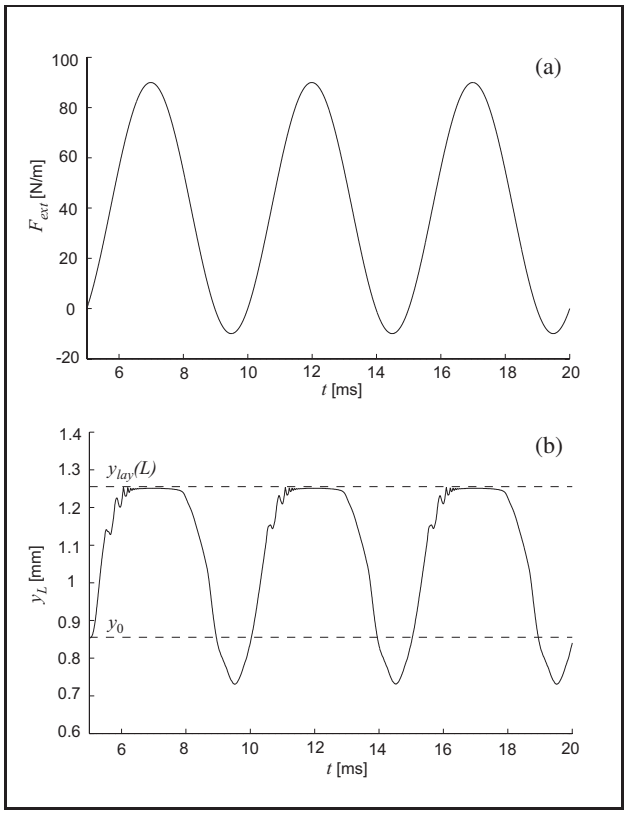

Figure 7. Dynamic simulations; (a) external driving force and (b) reed tip displacement.

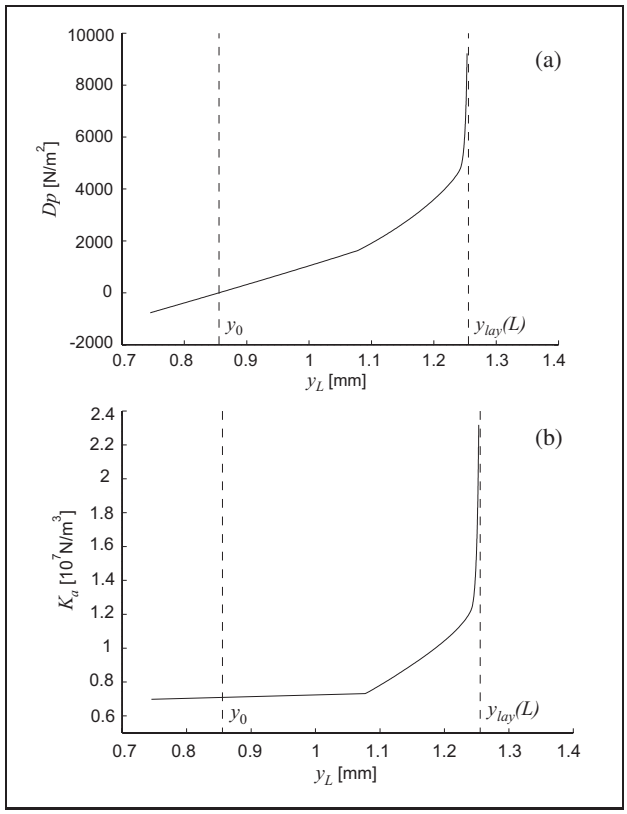

Figure 8. Quasi-static simulations: (a) pressure-displacement characteristics of the system and (b) stiffness per unit area K_a.

soidal force per unit length $(F_{ext})^n$ given by:

$$(F_{ext})^n = a_{min} + \left(\frac{a_{max} - a_{min}}{2}\right) \cdot \Big[1 + \sin\left(2\pi f_d\, nT_s + \phi_0\right)\Big], \qquad (20)$$

where ϕ_0 is such that $F_{ext} = 0$ for $n = 0$. The minimum and maximum amplitudes a_{min} and a_{max} were chosen in such a way that reed beating could be observed. Figure 7 shows the driving signal together with the corresponding tip displacement $y(L,t)$ as obtained from the simulations. These computed signals are qualitatively in agreement with findings by Idogawa et al. [21] on a real clarinet artificially blown. It is clearly seen that, due to interaction with the lay, the reed tip can not exceed the value $y_{lay}(L) = 1.3 \cdot 10^{-3}$ m. However, the tip is not stopped suddenly but rather gradually, and a zoom-in of the plot in Figure 7 in fact revealed that complete closure is not obtained. This suggests that the reed elastic properties are changing with increasing tip displacement. More precisely, the reed *stiffness per unit area* K_a is defined in [2] by

$$\Delta p = K_a(y_L - y_0), \qquad (21)$$

where $\Delta p = F_{ext}/w$ is the pressure acting on the reed and y_L, y_0 are the displacement and the rest position of the reed tip, respectively. The inverse of K_a is termed reed *compliance* by Nederveen [22]. Figure 7b thus suggests that K_a increases as y_L moves toward its maximum.

Table II. Analysis of convergence for f_1, with varying f_s and N. Frequency resolution in the FFT is 1.5 Hz, the f_1 values are rounded to the nearest integer.

		f_s (kHz)			
N	X_s (mm)	50	100	200	400
20	1.7	1361	1363	1364	1364
50	0.68	1387	1389	1390	1390
100	0.34	1397	1399	1401	1401
150	0.227	1400	1403	1404	1404
200	0.17	1402	1405	1405	1405
250	0.136	1403	1405	1407	1407
300	0.113	1403	1406	1407	1407
350	0.097	1404	1407	1407	1407
400	0.085	1405	1407	1408	1408

Another phenomenon which is evident from the same plot is that y_L exhibits small additional oscillations when approaching the maximum. In the next section an explanation is proposed for the occurrence of such oscillations, and quantitative results are provided about the dependence of K_a on tip displacement. However, dynamic simulations as defined above are not suitable for studying such a dependence, since the reed velocity can in principle induce hysteresis effects on the force-tip displacement character-

istics. Therefore, we resorted to *quasi-static* simulations, defined in the following way:

1. a constant driving force $(F_{ext})^n = a_{min}$ is applied to the system.
2. the computed reed displacement $\boldsymbol{y}^n$ is taken after n_0 samples. The length n_0 is taken such that the reed oscillations have decayed at this point.
3. the value of $(F_{ext})^n$ is increased by a small amount, and the procedure is iterated until $(F_{ext})^n = a_{max}$. This way the static displacement $\boldsymbol{y}^n$ is taken for a set of values of constant driving forces ranging from a_{min} to a_{max}.

5.3. Effects of reed curling

This section analyses the effect of reed curling up to the mouthpiece using quasi-static simulations. Figure 8 shows the dependence of the stiffness per unit area K_a as found from quasi-static simulations. As expected from the qualitative discussion in the last section, Figure 8a shows that the elastic behaviour of the system is approximately linear for small relative displacements, and becomes increasingly non-linear as the reed moves toward closure. Following equation (21), K_a is computed as the ratio between the driving pressure and the relative tip displacement, i.e. $K_a = \Delta p/(y_L - y_0)$. Figure 8b shows K_a versus y_L. Note that K_a is almost constant around y_0 and starts to increase significantly around the value $y_L \sim 1.08 \cdot 10^{-3}$ m. The additional oscillations observed in Figure 7b occur approximately in the same range. This findings suggest that the mechanical properties of the system are changing dramatically in that range.

In order to further investigate these changes, another numerical experiment was carried out in which the *separation point* x_{sep} (defined as the point of contact between lay and reed which is closest to the tip) was computed as a function of the reed tip displacement. The dependence $x_{sep}(y_L)$ describes the way the reed bends against the lay, and defines the part of the reed that can move freely during oscillation. Therefore it can be expected to be strongly correlated to the mechanical properties of the reed-mouthpiece system.

The separation point was first studied using quasi-static simulations. The computed values are plotted in Figure 9a, which shows an interesting result: the reed does not bend in a smooth manner, instead x_{sep} undergoes a sudden jump around $y_L \sim 1.08 \cdot 10^{-3}$ m. This behaviour corresponds to a reed section closer to the tip getting in contact with the lay before the "previous" segment has fully curled up onto the lay: Figure 9b gives a qualitative description of this behaviour.

Secondly, the separation point was studied using dynamic simulations. Several simulations were run using driving forces as in equation (20) with various f_d ranging from 200 Hz up to 1500 Hz. The grey dots in Figure 9a show results obtained with $f_d = 200$ Hz: slight hysteretic effects can be noticed, due to the fact that the opening and

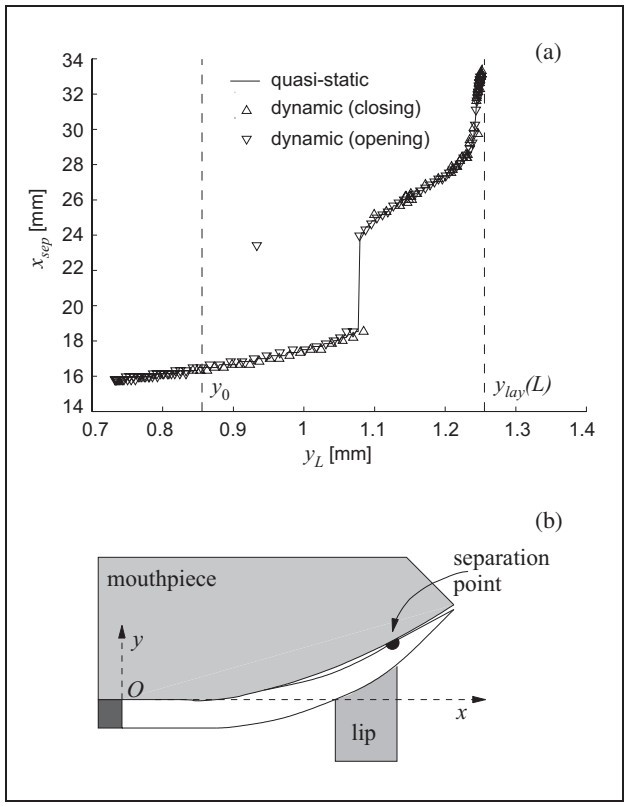

Figure 9. Separation point versus tip displacement; (a) quasi-static simulations (black solid line) and dynamic simulations with $f_d = 200$ Hz (grey dots); (b) non-smooth reed curling.

closing paths do not coincide exactly in dynamic simulations. However, the deviation from the static curve is generally small. Similar results were found for larger driving frequencies up to 1500 Hz. The behaviour depicted in Figure 9a is qualitatively in agreement with recent experimental results by Ollivier [23].

The separation point discontinuity explains the additional oscillations in tip displacement observed when running dynamical simulations (see Figure 7b). That is, at discontinuity a section of the reed hits the lay as depicted in Figure 9b, and the collision causes the free part to oscillate. Furthermore, the frequency of these oscillations is significantly higher than the first resonance f_1 of the reed. Qualitatively, this is explained by observing that at discontinuity the length of the reed segment which is moving freely is significantly smaller than the original length L.

In conclusion, the above analysis shows that quasi-static simulations provide an accurate description of reed motion, and can be used as an approximation of dynamic simulations.

6. Conclusions

In this paper we have proposed a distributed numerical model of the mechanical system formed by the single reed, the mouthpiece lay and the player's lip. In the development of the continuous-time model, attention has been focused

in particular on reed-lay and reed-lip interactions. Usual approaches in literature adopt simplified descriptions (for instance, collision of the reed with the lay is modelled by simply imposing geometrical constraints on reed displacement). Here it has been shown that these interactions can be treated in a physically consistent manner by introducing appropriate conditional contact forces.

Two main problems have been addressed for the accurate simulation of such a continuous system, namely the discretisation technique and the estimation of the physical parameters. As for the first issue, the finite-difference scheme presented in section 3 yields stable numerical simulations of the fourth-order reed equation; reformulating the lay and lip interactions in the digital domain required additional discussion. As for physical parameters, their values have been estimated via measurements on real instruments. For those parameters that are less easily established through direct measurements (e.g. lip damping or reed losses), a different strategy has been adopted, namely they have been "tuned" using numerical simulations.

The accuracy of the numerical system has been quantitatively assessed in section 5.1 through convergence analysis. This analysis has also driven the choice of the main numerical parameters, namely f_s, N, θ. Dynamic and quasi-static simulations have been analysed, showing that the behaviour of the numerical system is qualitatively in accordance with that observed in real instruments. In section 5.3 the effects of reed curling have been investigated: interestingly, it was observed that the reed does not bend in a smooth way, and that the separation point undergoes a discontinuity during reed bending. The consequences of this phenomenon on the system behaviour have been discussed.

However, these results hold for the specific geometry that we have chosen, i.e. a particular reed in combination with a particular lay shape and a fixed embouchure. Therefore, the general validity of these findings has to be assessed through numerical experiments that use different combinations of reed and lay geometries. Furthermore, the results presented here are exclusively based on numerical simulations, and comparisons with laboratory experiments on real reed-mouthpiece-lip systems are needed. Further research will be devoted to these issues.

The distributed model presented here may be employed as a numerical experimental tool. For example, one could use it to develop a lumped model approximation in which the lumped parameters vary with reed tip displacement. The results from such an application of the distributed model will be presented in a sequel to this paper.

Acknowledgments

The authors wish to thank Prof. D. M. Campbell for his help in the preparation of the manuscript, and Prof. J. P. Dalmont for his comments on a preliminary version of the paper. Two anonymous reviewers are also acknowledged for their insightful remarks.

Appendix

A1. Finite-difference scheme

For clarity, equation (1) is rewritten as

$$\begin{aligned} F(x,t) = \rho S(x)\left[\frac{\partial^2 y}{\partial t^2}(x,t) + \gamma_B \frac{\partial y}{\partial t}(x,t)\right] \\ + Y\frac{\partial^2}{\partial x^2}\left[I(x)\frac{\partial^2 y}{\partial x^2}(x,t)\right] \\ + \eta Y\frac{\partial^2}{\partial x^2}\left[I(x)\frac{\partial^3 y}{\partial x^2 \partial t}(x,t)\right], \end{aligned} \tag{A1}$$

and each of these derivative terms is addressed separately.

Time derivatives in equation (A1) are simply approximated using the centred difference scheme

$$\frac{\partial y}{\partial t}(x_i,t_n) \approx \frac{y_i^{n+1} - y_i^{n-1}}{2T_s}, \tag{A2}$$

$$\frac{\partial^2 y}{\partial t^2}(x_i,t_n) \approx \frac{y_i^{n+1} - 2y_i^n + y_i^{n-1}}{T_s^2}, \tag{A3}$$

The discrete operator δ_x^2, that approximates the second-order spatial derivatives, is again defined with a centred difference scheme. For a generic function $g(x)$

$$\frac{\partial^2 g}{\partial x^2} \approx \delta_x^2 g, \quad \text{where}$$

$$(\delta_x^2 g)_i^n = \frac{g_{i+1}^n - 2g_i^n + g_{i-1}^n}{X_s^2}. \tag{A4}$$

With this notation, the second-order derivative $\partial^2 y/\partial x^2$ is approximated as $\delta_x^2 y$ and the third-order derivative $\partial^3 y/\partial x^2 \partial t$ is approximated as

$$\frac{\partial^3 y}{\partial x^2 \partial t}(x_i,t_n) \approx \frac{(\delta_x^2 y)_i^{n+1} - (\delta_x^2 y)_i^{n-1}}{2T_s}. \tag{A5}$$

The θ-scheme approximates the fourth-order spatial derivative using the following three-level time average:

$$\begin{aligned} \frac{\partial^2}{\partial x^2}\left[I\frac{\partial^2 y}{\partial x^2}\right](x_i,t_n) \approx (1-2\theta)\delta_x^2[I(\delta_x^2 y)]_i^n \\ + \theta\left[\delta_x^2[I(\delta_x^2 y)]_i^{n+1} + \delta_x^2[I(\delta_x^2 y)]_i^{n-1}\right], \end{aligned} \tag{A6}$$

where $\delta_x^2[I(\delta_x^2 y)]_i^n$ can be written explicitly as

$$\begin{aligned} \delta_x^2\left[I(\delta_x^2 y)\right]_i^n = \frac{I_{i+1}y_{i+2}^n - 2(I_{i+1}+I_i)y_{i+1}^n}{X_s^4} \\ + \frac{(I_{i+1} + 4I_i + I_{i-1})y_i^n}{X_s^4} \\ + \frac{-2(I_i + I_{i-1})y_{i-1}^n + I_{i-1}y_{i-2}^n}{X_s^4}. \end{aligned} \tag{A7}$$

The last derivative in equation (A1) is again obtained using the θ-scheme. Substituting $\partial^3 y/\partial x^2 \partial t$ with its approxi-

mation (A5) and applying the θ-scheme (A6) yields

$$\frac{\partial^2}{\partial x^2}\left[I\,\frac{\partial^3 y}{\partial x^2 \partial t}\right](x_i,t_n) \approx \theta\, f_s\left[\delta_x^2[I(\delta_x^2 y)]_i^{n+1} - \delta_x^2[I(\delta_x^2 y)]_i^{n-1}\right]. \quad \text{(A8)}$$

Finally, extra grid-points have to be added at both ends, in order to express the boundary conditions (4) in discrete form. These turn out to be

$$\begin{aligned} y_0^n &= 0, \qquad y_{-1}^n = y_1^n, \\ y_{N+1}^n &= 2y_N^n - y_{N-1}^n, \\ y_{N+2}^n &= y_N^n - 4y_{N-1}^n + y_{N-2}^n. \end{aligned} \quad \text{(A9)}$$

Chaigne and Doutaut [14] exemplify the stability properties of this numerical scheme by applying it to the ideal bar equation $\partial^2 y/\partial t^2 = -a^2\partial^4 y/\partial x^4$. Their analytical study shows that *(1)* the difference equations are unconditionally stable for values $\theta \geq 1/4$ and that *(2)* minimum frequency warping is achieved by minimizing θ. Hence, $\theta = 1/4$ is the minimum value compatible with unconditional stability.

Note that Stewart and Strong [11] and Sommerfeldt and Strong [12] use a θ-scheme with $\theta = 1/2$, although they do not mention it explicitly.

References

[1] J. Backus: Small Vibration Theory of the Clarinet. J. Acoust. Soc. Am. **35** (1963) 305–313.

[2] W. E. Worman: Self-sustained Nonlinear Oscillations of Medium Amplitude in Clarinet-like Systems. Dissertation. Case Western Reserve university, Cleveland, OH, 1971.

[3] M. E. McIntyre, R. T. Schumacher, J. Woodhouse: On the Oscillations of Musical Instruments. J. Acoust. Soc. Am. **74** (1983) 1325–1345.

[4] N. H. Fletcher: Mode Locking in Nonlinearly Excited Inharmonic Musical Oscillators. J. Acoust. Soc. Am. **64** (1978) 1566–1569.

[5] T. A. Wilson, G. S. Beavers: Operating modes of the clarinet. J. Acoust. Soc. Am. **56** (1974) 653–658.

[6] R. T. Schumacher: *Ab Initio* Calculations of the Oscillations of a Clarinet. Acustica **48** (1981) 71–85.

[7] A. Hirschberg, R. W. A. van de Laar, J. P. Marrou-Mauriéres, A. P. J. Wijnands, H. J. Dane, S. G. Kruijswijk, A. J. M. Houtsma: A Quasi-stationary Model of Air Flow in the Reed Channel of Single-reed Woodwind Instruments. Acustica **70** (1990) 146–154.

[8] A. Hirschberg: Aero-acoustics of wind instruments. – In: The Mechanics of Musical Instruments. A. Hirschberg, J. Kergomard, G. Weinreich (eds.). Springer-Verlag, New York, 1995.

[9] J. Gilbert: Etude des instruments de musique à anche, simple: extension de la méthode d'équilibrage harmonique, rôle de l'inharmonicité des résonances, mesure des grandeurs d'entrée. Dissertation. Laboratoire d'Acoustique de l'Université du Maine, Le Mans, France, 1991.

[10] J. P. Dalmont, J. Gilbert, S. Ollivier: Non-linear characteristics of single reed instruments: quasi-static volume flow and reed opening measurements. J. Acoust. Soc. Am. (2003). Submitted for publication.

[11] S. E. Stewart, W. J. Strong: Functional model of a simplified clarinet. J. Acoust. Soc. Am. **68** (1980) 109–120.

[12] S. D. Sommerfeldt, W. J. Strong: Simulation of a player-clarinet system. J. Acoust. Soc. Am. **83** (1988) 1908–1918.

[13] B. Gazengel: Caractérisation objective de la qualité de justesse, de timbre et d'émission des instruments à vent, à anche, simple. Dissertation. Laboratoire d'Acoustique de l'Université du Maine, Le Mans, France, 1994.

[14] A. Chaigne, V. Doutaut: Numerical Simulations of Xylophones. I. Time-domain Modeling of the Vibrating Bar. J. Acoust. Soc. Am. **101** (1997) 539–557.

[15] E. Ducasse: Modèlisation et simulation dans le domaine temporel d'instrument à vent à anche simple en situation de jeu: méthodes et modèls. Dissertation. Ecole Nationale Superieure d'Arts et Metiers, Bordeaux, France, 2001.

[16] M. Facchinetti, X. Boutillon, A. Constantinescu: Numerical and experimental modal analysis of the reed and pipe of a clarinet. J. Acoust. Soc. Am. (2003). Submitted for publication.

[17] M. Roseau: Vibrations in mechanical systems: analytical methods and applications. Springer-Verlag, Berlin, 1987.

[18] P. M. Morse, K. U. Ingard: Theoretical acoustics. Princeton University Press, Princeton, New Jersey, 1968.

[19] L. Lapidus, G. Pinder: Numerical solution of partial differential equations in science and engineering. John Wiley & Sons, New York, 1982.

[20] S. C. Thompson: The effect of the reed resonance on woodwind tone production. J. Acoust. Soc. Am. **66** (1979) 1299–1307.

[21] T. Idogawa, T. Kobata, K. Komuro, M. Iwaki: Nonlinear Vibrations in the Air Column of a Clarinet Artificially Blown. J. Acoust. Soc. Am. **93** (1993) 540–551.

[22] C. J. Nederveen: Acoustical Aspects of Woodwind Instruments. F. Knuf, Amsterdam, 1969.

[23] S. Ollivier: Contribution a l'etude des oscillations des instruments à vent à anche simple. validation d'un modele elementaire. Dissertation. Laboratoire d'Acoustique de l'Université du Maine, Le Mans, France, 2003.